



Distortion of the perfect lattice structure in bilayer graphene

Vitor M. Pereira

Department of Physics, Boston University, 590 Commonwealth Avenue, Boston, Massachusetts 02215, USA

R. M. Ribeiro and N. M. R. Peres

Department of Physics and Center of Physics, University of Minho, P-4710-057 Braga, Portugal

A. H. Castro Neto

Department of Physics, Boston University, 590 Commonwealth Avenue, Boston, Massachusetts 02215, USA

(Received 2 October 2008; revised manuscript received 18 December 2008; published 27 January 2009)

We consider the instability of bilayer graphene with respect to a distorted configuration in the same spirit as the model introduced by Su *et al.* [Phys. Rev. Lett. **42**, 1698 (1979)]. By computing the total energy of a distorted bilayer, we conclude that the ground state of the system favors a finite distortion. We explore how the equilibrium configuration changes with carrier density and an applied potential difference between the two layers.

DOI: [10.1103/PhysRevB.79.045421](https://doi.org/10.1103/PhysRevB.79.045421)

PACS number(s): 81.05.Uw, 71.18.+y, 71.15.Nc

I. INTRODUCTION

A planar arrangement of carbon atoms covalently bound via sp^2 orbitals exhibits a honeycomb structure and is denoted graphene. Graphene rose rapidly to the forefront of research in condensed-matter physics mostly because of the peculiar electronic structure that emerges from its crystalline arrangement and the consequent wealth of rich and unexpected phenomena.¹ Seminal experiments on two-dimensional crystals established graphene as an accessible reality,² and immediately unveiled numerous surprises, both on a fundamental level—like a new form of quantized Hall effect—and on a practical and technological level—like the highly efficient field effect and high electronic mobility.^{3,4} Most of the appealing phenomenology of graphene owes to the fact that electron dynamics in this system can be described in terms of chiral massless Dirac fermions,³ and, in fact, graphene does exhibit many properties characteristic of relativistic particles.^{5,6}

Equally remarkable phenomena occur in bilayer graphene, which consists of two adjacent graphene planes stacked in the A-B fashion, typical of graphite. Bilayer graphene displays the same sample quality and quasiballistic transport characteristic of its single-layer counterpart,⁷ but brings also its share of new physics stemming from the nature of its charge carriers: chiral massive electrons.⁸ Most interesting is the fact that, although gapless in its pristine form, a potential difference between the two layers opens a gap in the spectrum that can be controlled via chemical doping⁹ or gating.^{10–12}

Despite such favorable prospects, the amount of knowledge gathered in the context of bilayer graphene still lags behind the intensity committed to single-layer graphene. In this paper, we address a particular aspect of the electron-phonon interaction in bilayer graphene, namely, the tendency to relax the perfect crystal structure and generate a static uniform deformation. This effect is inspired and similar in spirit to the well-known Peierls instability that occurs in polyacetylene chains. As shown by Su, Schrieffer, and Hee-

ger (SSH),^{13,14} in polyacetylene the one-dimensional chain of carbon atoms has a half-filled electronic ground state that is unstable with respect to a spontaneous dimerization. This dimerization opens a sizeable gap in the spectrum that can be easily detected experimentally.¹⁵

The instability we envisage for bilayer graphene is related with the application of the ansatz of SSH to the interplane hopping, t_{\perp} . From the outset, the atoms lying in the A and B sublattices within each layer are not equivalent since only one of the sublattices connects to the adjacent plane (Fig. 1). This has important experimental consequences: one example is the known fact that in tunneling experiments one typically detects only one of the sublattices of the topmost layer.¹⁶ In the absence of a potential difference between the two layers (unbiased situation), the bilayer is a zero gap semiconductor, with hyperbolic bands touching at the Fermi energy (Fig. 1). A change in the interlayer hopping will not change this situ-

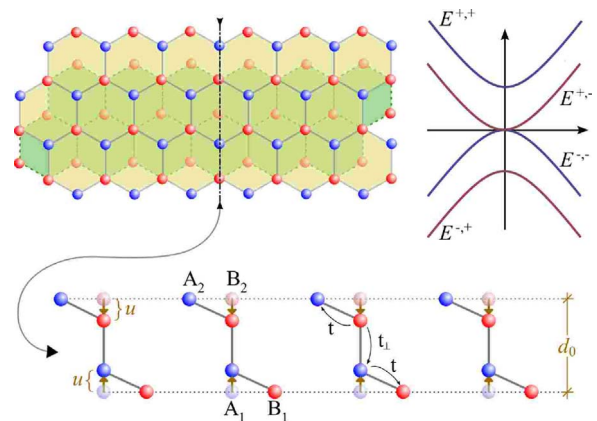


FIG. 1. (Color online) Transverse view (bottom) along the dashed-dotted line (top left) of the lattice distortion considered in the text. Only the atoms A_1 and B_2 , which are connected via the hopping t_{\perp} , are displaced toward each other in the distorted phase. The vertical displacement of the carbon atoms connected by t_{\perp} is represented by the parameter u . In the top right we schematically represent the band structure in the vicinity of the Dirac point.

ation, and thus the gap can still be tuned through the potential difference between layers. However, as shown below, the electron-phonon interaction might, indeed, lead to a stable distorted configuration.

II. MODEL

A. Tight-binding description of a biased bilayer

The electronic Hamiltonian of a biased bilayer consists of two contributions, $H_e = H_{\text{tb}} + H_V$, where H_{tb} is the tight-binding Hamiltonian for the graphene bilayer and H_V reflects the electrostatic bias applied between the two graphene planes. The tight-binding Hamiltonian H_{tb} is comprised of three terms describing electron itinerancy among each individual plane and between the two planes. In detail we have

$$H_{\text{tb}} = H_{\text{tb1}} + H_{\text{tb2}} + H_{\perp}, \quad (1)$$

with

$$H_{\text{tb1}} = -t \sum_{\mathbf{R}, \sigma} [a_{1\sigma}^{\dagger}(\mathbf{R})b_{1\sigma}(\mathbf{R}) + a_{1\sigma}^{\dagger}(\mathbf{R})b_{1\sigma}(\mathbf{R} - \mathbf{a}_1) + a_{1\sigma}^{\dagger}(\mathbf{R})b_{1\sigma}(\mathbf{R} - \mathbf{a}_2) + \text{H.c.}], \quad (2)$$

$$H_{\text{tb2}} = -t \sum_{\mathbf{R}, \sigma} [a_{2\sigma}^{\dagger}(\mathbf{R})b_{2\sigma}(\mathbf{R}) + a_{2\sigma}^{\dagger}(\mathbf{R} + \mathbf{a}_1)b_{2\sigma}(\mathbf{R}) + a_{2\sigma}^{\dagger}(\mathbf{R} + \mathbf{a}_2)b_{2\sigma}(\mathbf{R}) + \text{H.c.}], \quad (3)$$

$$H_{\perp} = -t_{\perp} \sum_{\mathbf{R}, \sigma} [a_{1\sigma}^{\dagger}(\mathbf{R})b_{2\sigma}(\mathbf{R}) + b_{2\sigma}^{\dagger}(\mathbf{R})a_{1\sigma}(\mathbf{R})], \quad (4)$$

and

$$H_V = \frac{V}{2} \sum_{\mathbf{R}, \sigma} [a_{1\sigma}^{\dagger}(\mathbf{R})a_{1\sigma}(\mathbf{R}) + b_{1\sigma}^{\dagger}(\mathbf{R})b_{1\sigma}(\mathbf{R})] - \frac{V}{2} \sum_{\mathbf{R}, \sigma} [a_{2\sigma}^{\dagger}(\mathbf{R})a_{2\sigma}(\mathbf{R}) + b_{2\sigma}^{\dagger}(\mathbf{R})b_{2\sigma}(\mathbf{R})]. \quad (5)$$

In the above equations \mathbf{a}_1 and \mathbf{a}_2 represent the elementary translations of the honeycomb lattice. In the presence of an electrostatic bias, V , the electronic dispersion is given by the four branches

$$E_{\mathbf{k}}^{\pm, \pm} = \pm \frac{1}{2} \sqrt{2t_{\perp}^2 + V^2 + 4t^2|\phi_{\mathbf{k}}|^2 \pm \Delta_{\mathbf{k}}}, \quad (6)$$

where

$$\Delta_{\mathbf{k}} = 2\sqrt{t_{\perp}^4 + 4t^2(t_{\perp}^2 + V^2)|\phi_{\mathbf{k}}|^2}. \quad (7)$$

When $V=0$ Eq. (6) simplifies to

$$E_{\mathbf{k}}^{\pm, \pm} = \pm \frac{1}{2} (\pm t_{\perp} + \sqrt{t_{\perp}^2 + 4t^2|\phi_{\mathbf{k}}|^2}), \quad (8)$$

where $\phi_{\mathbf{k}}$ is associated with the dispersion of a single layer, and is given by

$$\phi_{\mathbf{k}} = 1 + e^{i\mathbf{k} \cdot \mathbf{a}_1} + e^{i\mathbf{k} \cdot \mathbf{a}_2}. \quad (9)$$

In order to proceed analytically we consider the effective band structure that follows from the low-energy expansion

around the Fermi points \mathbf{K} and \mathbf{K}' in the Brillouin zone (BZ).¹ We approximate $|\phi_{\mathbf{k}}|$ by

$$|\phi_{\mathbf{k}}| \approx \frac{3}{2}aq, \quad (10)$$

where a represents the in-plane carbon-carbon distance, and we took $\mathbf{k} = \mathbf{K} + \mathbf{q}$, with q assumed to be small compared with \mathbf{K} . This procedure amounts to using the effective-mass approximation for bilayer graphene. The resulting band structure is depicted in Fig. 1.

B. Parametrization of distortion

We consider a distortion of the perfect lattice structure of the bilayer, such that the A and the B atoms in different planes, connected by the hopping parameter t_{\perp} , distort along the vertical direction by an amount u_i (Fig. 1). In the spirit of the SSH model for polyacetylene¹⁴ we assume that, to leading order in the deformation, the effect of this distortion is to change the value of t_{\perp} according to

$$t_{\perp} = t_{\perp}^0 (1 + \alpha u_i), \quad (11)$$

where t_{\perp}^0 is the value of the interlayer hopping of the undistorted lattice. The case with $u_i=0$ corresponds to the absence of any distortion so that all atoms in each plane lie at a distance d_0 from the adjacent plane (Fig. 1). In our convention, when $u_i > 0$ the neighboring atoms in the different planes approach each other. For small u_i the in-plane hopping t is affected by this distortion only at higher orders in u_i , and therefore we neglect its variation. This distortion will naturally induce an elastic restoring force that we parametrize through the term

$$H_{\text{el}} = K \sum_{i=1}^{N_c} u_i^2 + \sum_{i=1}^{N_c} \frac{P_i^2}{M}, \quad (12)$$

N_c denoting the number of unit cells. In the static and homogeneous situation represented in Fig. 1 the kinetic term gives an average null contribution, and all u_i acquire the same mean value: $u_i = u$. This is the phase that we study throughout the remainder of the paper: a uniform distortion that affects the distance between the atoms connected by t_{\perp} only. The total elastic energy for the distorted phase reads

$$E_{\text{el}} = K \sum_{i=1}^{N_c} u^2 = KN_c u^2. \quad (13)$$

The stability analysis of such a distorted phase proceeds by minimization of the total electronic and elastic energy, given by $H_e + H_{\text{el}}$, with respect to the distortion u . We underline the fact that, unlike in the original polyacetylene model,¹⁴ parametrization (11) does not change the original periodicity of the lattice. The unit cell remains the same, and since it only affects t_{\perp} , the gapless (unbiased) or gapped (biased) character of the spectrum remains unaltered. Therefore this distortion does not require a density commensurability to be effective.

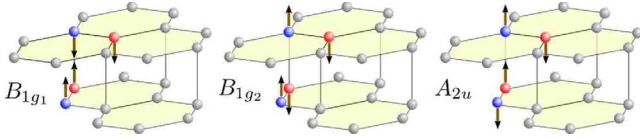


FIG. 2. (Color online) Phonon modes along the c axis in graphite, using the notation of Ref. 17. The modes A_{2u} and B_{1g_2} are nearly degenerate at the center of the Brillouin zone, with $\omega \approx 870 \text{ cm}^{-1}$ (Refs. 17 and 18).

C. Estimation of parameters

A precise estimation of the parameters required for the computation of the stable distorted configuration is neither easy nor unique. On the one hand, little is known with respect to the structural and elastic properties of a graphene bilayer, and thus we will rely on the corresponding knowledge that exists for graphite. On the other hand, details such as the type of substrate can significantly alter these parameters, as happens, for instance, with the phonon spectrum that can be sensitive to substrate and other constraints in the system.

We will therefore resort to the structural parameters (lattice constant and elastic coefficients) known for A-B stacked graphite. The carbon-carbon distance is $a \approx 1.42 \text{ \AA}$, and the graphene unit cell has an area given by $A_c = 3\sqrt{3}a^2/2$. The equilibrium interlayer distance is given by $d_0 = c_0/2 \approx 3.35 \text{ \AA}$, and corresponds to half the unit-cell height of A-B stacked graphite.¹⁹⁻²¹

The value of the stiffness, K , can be estimated from the phonon spectrum of graphite. In particular the B_{1g_2} optical (out-of-plane) phonon mode has a frequency of $\omega \approx 870 \text{ cm}^{-1}$, which is seen both experimentally²² and from *ab-initio* calculations.¹⁸ As a result of the weak interlayer interaction, this phonon is essentially degenerate with the out-of-plane phonon A_{2u} present in a single layer of graphene. These normal modes are represented in Fig. 2. We can assume that K relates to this frequency through $Ka^2 \sim m\omega^2 a^2/4$, where m is the carbon atom mass.²³ As a result we obtain an estimate for the stiffness $K \approx 8.5 \text{ eV \AA}^{-2}$.

With respect to the electron-phonon coupling α , its estimation is most straightforward from the knowledge of how the interplane hopping varies with distance. The interplane hopping t_\perp corresponds to the tight-binding parameter $V_{pp\sigma}$ in the two-center Slater-Koster formalism.^{24,25} For instance, assuming that

$$V_{pp\sigma}(r) \approx Ae^{-\alpha r} \quad (14)$$

one can extract α from interpolation of the hopping γ_1 and the in-plane $V_{pp\sigma}(a)$ for graphite. Using the values^{17,26} $\gamma_1 \approx 0.4 \text{ eV}$ and $V_{pp\sigma}(a) \approx 3.7 \text{ eV}$ we obtain $\alpha \approx 1.2 \text{ \AA}^{-1}$. Alternatively to formula (14), one could use a more refined interpolation formula for $V_{pp\sigma}(r)$ as discussed in Ref. 27. This yields $\alpha \approx 1.8 \text{ \AA}^{-1}$, consistent with the previous estimate.

Finally, several recent experiments on the bilayer²⁸⁻³⁰ show that the value of t_\perp^0 is essentially the value expected in graphite, $t_\perp^0 \approx 0.3 \text{ eV}$, the same applying to the in-plane hopping, $t \approx 3 \text{ eV}$.

III. AB INITIO CALCULATION OF THE ELASTIC CONSTANT

In addition to the above estimates of the model parameters, we have extracted the compression elastic constant from a first-principles calculation. Density-functional calculations in graphite and related compounds must be carried out with caution for it is known that different implementations of density-functional theory can yield noticeably different results.^{18,31} Having this in mind, we calculated the equilibrium distance between graphene planes in the bilayer by resorting to two different approximations: the generalized gradient approximation (GGA) and the local-density approximation (LDA).

For GGA we used the scheme proposed by Perdew, Burke, and Ernzerhof,³² with a grid of $12 \times 12 \times 4 \mathbf{k}$ points. Bilayer graphene was modeled in a slab geometry by including a vacuum region in a supercell containing four carbon atoms (two for each graphene sheet). In the normal direction (z direction) the vacuum separating repeating slabs has more than 10 \AA , and the size of the supercell in the z direction was optimized to make sure there was no interaction between repeating slabs. The Gaussian basis set and k -point grid were likewise optimized.

In the LDA case the BZ was sampled according to the scheme proposed by Monkhorst and Pack,³³ with a grid of $4 \times 4 \times 1 \mathbf{k}$ points, and using a supercell comprising eight carbon atoms (four for each sheet). Adjacent slabs along the z direction were separated by more than 30 \AA , and the size of the supercell along this direction was again optimized.

In either case an increase in the number of sampling points did not result in a significant total-energy change, and the vertical separation quoted above guarantees the absence of interaction between adjacent slabs. We used dual-space separable pseudopotentials by Hartwigsen, Goedecker, and Hutter³⁴ to describe the ion cores. In a first step, all the atoms were fully relaxed to their equilibrium positions. Then one of the graphene sheets was moved as a whole in the z direction by very small displacements, and the total energy of the system was calculated, without any further relaxation.

Figure 3 shows the GGA variation in the total energy relative to the relaxed sample, as a function of the displacement from the equilibrium position. Also shown is the parabola that was fitted to the calculated values. The fitting gave a value of $K = 0.615 \pm 0.002 \text{ eV/\AA}^2$ per unit cell. The same calculation within LDA yields $K = 4.15 \pm 0.06 \text{ eV/\AA}^2$. The two calculations therefore differ by a considerable amount. This is related to the fact that in our calculations the equilibrium distance between the two graphene planes is different in the two DFT schemes used. The GGA consistently yields a higher value for d_0 , which, in turn, has an effect on the compressive stiffness. These discrepancies signal that, like in other systems derived from graphite, density-functional calculations are very sensitive to the details of the approximation used. This is particularly pressing and more evident in quantities directly related to the interlayer coupling, which, having a van der Waals nature, is difficult to capture within DFT.

IV. TOTAL ENERGY AT CONSTANT μ

Our main objective is to quantify the equilibrium distortion that is expected to emerge from the competition between

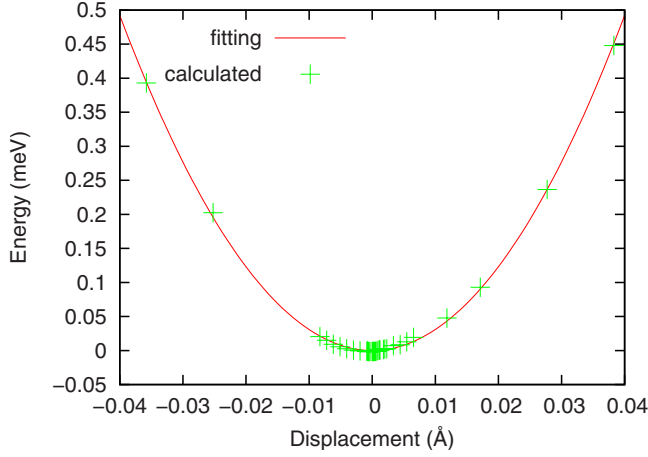


FIG. 3. (Color online) Energy as a function of distance between layers measured with respect to the equilibrium position, and calculated within the GGA. The positive direction indicates a displacement toward the other graphene sheet. The zero-value energy is the energy of the fully relaxed sample.

elastic and electronic energies in the ground state. For illustration purposes we consider first the computation of the total energy in the (potentially artificial) case where the chemical potential is held constant. In particular, we assume that the density of carriers in the bilayer is such that the chemical potential is located between $E_{q=0}^{+,+}$ and $E_{q=0}^{+,-}$,

$$\mu = \frac{V + \sqrt{V^2 + 4t_{\perp}^2}}{4}. \quad (15)$$

Let us start with an unbiased bilayer ($V=0$). In this case the total electronic energy per unit cell is given by

$$\frac{E_e}{N_c} = \frac{gA_c}{2\pi} \int_0^{q_c} dq q (E_q^{+,+} + E_q^{+,-}) + \frac{gA_c}{2\pi} \int_0^{q_F} dq q E_q^{+,-}. \quad (16)$$

The integral is elementary leading to

$$\begin{aligned} \frac{E_e}{N_c} = & \frac{gA_c}{2\pi} t_{\perp} \left(\frac{q_t^2}{6} - \frac{q_F^2}{4} \right) - \frac{gA_c}{6\pi} t_{\perp} q_t^2 \left[1 + \left(\frac{q_c}{q_t} \right)^2 \right]^{3/2} \\ & + \frac{gA_c}{12\pi} t_{\perp} q_t^2 \left[1 + \left(\frac{q_F}{q_t} \right)^2 \right]^{3/2}, \end{aligned} \quad (17)$$

where the momenta q_F , q_c , and q_t are defined as

$$q_t = \frac{t_{\perp}}{3ta}, \quad q_c = \sqrt{\frac{2\pi}{A_c}}, \quad q_F = \frac{\sqrt{(2\mu + t_{\perp})^2 - t_{\perp}^2}}{3ta}, \quad (18)$$

and $A_c = 3\sqrt{3}a^2/2$ is the area of the graphene unit cell. The total energy E_t per unit cell is given by

$$\frac{E_t}{N_c} = \frac{E_e}{N_c} + Ku^2. \quad (19)$$

These two terms compete in such a way that the minimum-energy state is achieved for a finite value of u .

The dashed lines of the top panels of Fig. 4 represent the total energy, E_t , as a function of the deformation u , using different values of the stiffness parameter, K . It is also in-

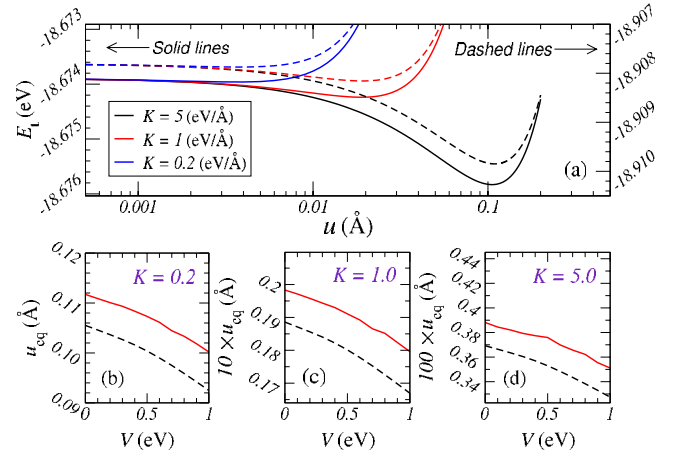


FIG. 4. (Color online) (a) Total energy, E_t , per unit cell as a function of the deformation parameter u , and for different values of K . The left (right) vertical axis pertains to the solid (dashed) curves. [(b)–(d)] The equilibrium radius as a function of the bias voltage, V . In all panels dashed lines refer to the Dirac approximation, whereas full lines have been calculated using the full tight-binding dispersion in Eq. (6). Notice that in panels (c) and (d) the vertical axis is amplified ten and 100 times, respectively. Other parameters used are $t_{\perp}^0 = 0.3$ eV, $t = 3.0$ eV, $\alpha = 1.5$ Å⁻¹.

structive to investigate to what extent approximation (10) influences the equilibrium deformations, and for that, we have performed the calculation of the total energies using the full tight-binding dispersions of Eq. (6). The results so obtained are represented in the same figure by the solid lines. It is clear from Fig. 4(a) that, besides yielding slightly larger absolute values for the energy, the full dispersion increases the equilibrium deformation by about 5 to 10%.

The analytical calculation in the presence of a finite bias ($V \neq 0$) is also straightforward. The total energy is still given by Eq. (16), where $E_k^{\pm,\pm}$ is now given by Eq. (6). The energy integrals are given in Appendix B, the final result being

$$\frac{E_{el}}{N_c} = \frac{gA_c}{2\pi} [F^{-,+}(k)|_0^{q_c} + F^{-,-}(k)|_0^{q_c} + F^{+,-}(k)|_0^{q_F}]. \quad (20)$$

The primitives $F^{\eta_1,\eta_2}(k)$ are calculated in Appendix B, with the final result

$$\begin{aligned} F^{\eta_1,\eta_2}(k) = & \frac{\eta_1}{8\nu_F^2(t_{\perp}^2 + V^2)} \left\{ \frac{R^{3/2}}{3\gamma} - \frac{\gamma x + \eta_2}{2\gamma^2} \eta_2 \sqrt{R} \right. \\ & \left. - \frac{\eta_2 \Delta}{8\gamma^{5/2}} \log(2\sqrt{\gamma R} + 2\gamma x + 2\eta_2) \right\}, \end{aligned} \quad (21)$$

and the remaining parameters are defined in Eq. (B5).

Placing the chemical potential again at the midpoint between the two conduction bands at $q=0$ [Eq. (15)] the corresponding Fermi wave vector is

$$q_F = \frac{1}{2\nu_F} \sqrt{V^2 + 4\mu + 2\sqrt{4\mu(t_{\perp}^2 + V^2) - t_{\perp}^2 V^2}}, \quad (22)$$

and we obtain the results shown in the lower panel of Fig. 4 for the equilibrium radius. When V varies between 0 and 1

eV, the equilibrium radius shows a relative variation of $\sim 15\%$. In addition, it can be seen that the difference between using the Dirac approximation and the full tight-binding dispersion is, in accordance with the above, essentially a systematic increase in the equilibrium radius. For this reason, henceforth we will restrict the discussion to the results obtained within the Dirac approximation, in which case all calculations can be carried out analytically.

V. TOTAL ENERGY AT CONSTANT n_e

We consider now the more relevant case of a bilayer with constant carrier density, which can be tuned, for instance, through a gate voltage. We define n_e as the number of electrons per unit cell, with respect to the charge-neutral situation in which the valence bands are fully occupied. In addition we will be concerned with electron doping only. The calculation of the electronic energy in this case requires, in general, the consideration of three distinct possibilities. Assuming a biased situation, and with respect to the notation defined in Fig. 7, we can have

(i) the Fermi level lying between E_1 and E_2 , in which case the Fermi surface consists of a Fermi ring characterized by two Fermi momenta $q_F^{\text{III},1}$ and $q_F^{\text{III},2}$, and the phase space exhibits a central hollow;

(ii) the Fermi level lying between E_2 and E_3 , where we have a more conventional Fermi surface;

(iii) the Fermi level lying above the bottom of the uppermost band, in which case we have again two Fermi momenta, q_F^{III} and q_F^{IV} , but the phase space is now simply connected.

The boundaries of these regimes can be easily identified through the two threshold densities

$$n_e^* = \frac{gA_c}{4\pi} q_2^2 \quad \text{and} \quad n_e^{**} = \frac{gA_c}{4\pi} q_3^2. \quad (23)$$

It follows that the total electronic energy is computed as

$$\begin{aligned} \frac{E_e}{N_c} = & \frac{gA_c}{2\pi} \int_0^{q_c} q dq (E_q^{+,-} + E_q^{-,-}) \\ & + \frac{gA_c}{2\pi} \int_{q_F^{\text{III},1}}^{q_F^{\text{III},2}} q dq E_q^{+,-} + \frac{gA_c}{2\pi} \int_0^{q_F^{\text{IV}}} q dq E_q^{+,+}, \end{aligned} \quad (24)$$

where the integration limits of the last two terms are given by (see also Fig. 7 for notation)

$$(i) \quad n_e < n_e^*: \quad (25a)$$

$$q_F^{\text{IV}} = 0,$$

$$\begin{aligned} \left\{ \begin{aligned} n_e = & \frac{gA_c}{4\pi} [(q_F^{\text{III},2})^2 - (q_F^{\text{III},1})^2] \\ & 2\nu_F^2 (q_F^{\text{III},1})^2 - \sqrt{t_\perp^4 + 4\nu_F^2 (q_F^{\text{III},1})^2 (t_\perp^2 + V^2)} \end{aligned} \right. \\ = & 2\nu_F^2 (q_F^{\text{III},2})^2 - \sqrt{t_\perp^4 + 4\nu_F^2 (q_F^{\text{III},2})^2 (t_\perp^2 + V^2)}. \end{aligned}$$

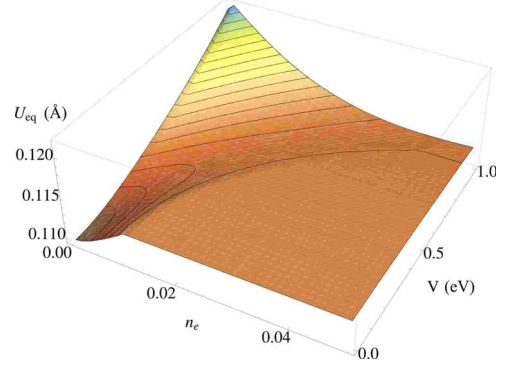


FIG. 5. (Color online) Equilibrium deformation, u_{eq} , as a function of the electron density per unit cell (n_e) and the bias voltage (V). The lines drawn on the surface represent level curves. The parameters used are $t_\perp^0 = 0.3$ eV, $t = 3.0$ eV, $K = 0.2$ eV \AA^{-2} , and $\alpha = 1.5$ \AA^{-1} .

$$(ii) \quad n_e^* < n_e < n_e^{**}: \quad (25b)$$

$$q_F^{\text{IV}} = 0,$$

$$q_F^{\text{III},1} = 0,$$

$$q_F^{\text{III},2} = \frac{gA_c}{4\pi} \left(\frac{1}{n_e} \right)^{-1/2}.$$

$$(iii) \quad n_e > n_e^{**}: \quad (25c)$$

$$q_F^{\text{III},1} = 0,$$

$$\begin{aligned} \left\{ \begin{aligned} n_e = & \frac{gA_c}{4\pi} [(q_F^{\text{III},2})^2 + (q_F^{\text{IV}})^2] \\ & 2\nu_F^2 (q_F^{\text{III},2})^2 + \sqrt{t_\perp^4 + 4\nu_F^2 (q_F^{\text{III},2})^2 (t_\perp^2 + V^2)} \end{aligned} \right. \\ = & 2\nu_F^2 (q_F^{\text{IV}})^2 - \sqrt{t_\perp^4 + 4\nu_F^2 (q_F^{\text{IV}})^2 (t_\perp^2 + V^2)}. \end{aligned}$$

Minimizing the total energy with respect to u yields the equilibrium displacements plotted in Fig. 5, for different electron densities and bias voltages. The typical deformations for the parameters quoted in the figure are ~ 0.11 \AA , which represents $\sim 8\%$ of the carbon-carbon distance, a . The variation in u_{eq} with n_e and V is nonmonotonic. In particular, one notices that for constant V , the equilibrium deformation tends to saturate beyond a given density. This can be appreciated in more detail in Fig. 6(a), where we present selected cuts of the same surface. The saturation can be understood from the interplay of two factors: on one hand, the variation in V and n_e induces changes in the band structure only in a region close to the neutrality point; on the other hand, for high enough density, the Fermi level will always be considerably above the bottom of the uppermost band (E_3 in Fig. 7). In fact, comparing the values of n_e^* and n_e^{**} presented in Fig. 6(b), one can verify that the first sets the scale for the minimum in the curves of u_{eq} versus n_s , therefore defining

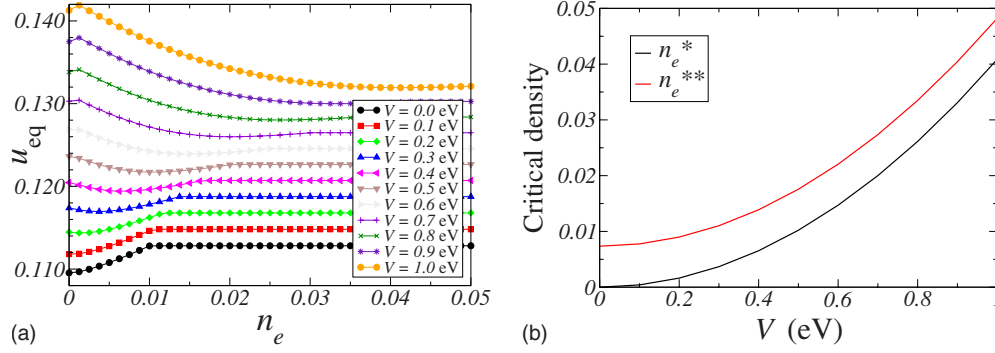


FIG. 6. (Color online) (a) Selected cuts from Fig. 5 at constant bias V . For clarity, successive curves have been shifted vertically by 0.002 in the order of increasing V . (b) The densities n_e^* and n_e^{**} defined in Eq. (23), plotted as a function of V for the same parameters used in Fig. 5.

the shape of the valley in the plot of Fig. 5. The value n_e^{**} , on the other hand, marks the onset of saturation.

VI. DISCUSSION AND CONCLUSIONS

By comparing the results obtained with the full tight-binding dispersion of bilayer graphene with the effective-mass approximation [Figs. 4(c)–4(e)], we concluded that the former does not introduce significant changes in the equilibrium results, and therefore the low-energy approximation is adequate to study this instability.

The deformation of the perfect planar arrangement of the carbon atoms in each plane can have measurable consequences. On one hand, if the lattice structure relaxes as seen here, the effect can be detected by means of standard diffraction probes. On the other hand, the distortion leads to the renormalization of the interplane hopping, t_{\perp} , through Eq. (11). This might lead to noticeable spectroscopic signatures, examples of which are changes in the band curvature, measurable via angle-resolved photoemission spectroscopy; changes in Landau-level separation, measurable via cyclotron resonance experiments; and shift of resonant frequencies for optical absorption.

For the values of K used in Fig. 5, the magnitude of the deformation corresponds to roughly 10% of the in-plane carbon-carbon distance, and is significant. However, at this point one can hardly be definite about a specific value of the equilibrium deformation on account of the uncertainties in the estimation of the parameters K and α . The value used for K is close to the compressive stiffness found with the GGA calculation described above. But clearly, had we used the estimate for the phonon B_{1g_2} (or the LDA result) instead, we would have obtained much smaller values of u_{eq} , as can be inferred from Fig. 4(d), although the qualitative features of Fig. 5 would be preserved. Hence a definitive conclusion as to the magnitude of the effect is deferred until the relevant parameters in bilayer graphene are experimentally available.

In the consideration of the electronic energy, we have accounted only for nearest-neighbor in-plane and interplane hoppings. Additional hopping terms, such as next-nearest-neighbor and other interplane hoppings, should not change the qualitative picture presented here (this follows because

additional hopping terms will not change the fact that the electronic energy decreases when neighboring atoms approach each other). On a quantitative level, even the additional hoppings that are affected in first order in u are expected to contribute only slightly on account of their smaller magnitudes in comparison with t and t_{\perp} . Electron-electron interactions have also been neglected. This is justified, in first approximation, by the results of Ref. 35, which, at the Hartree-Fock level, show that electron-electron interactions lead to the same band structure, albeit with renormalized parameters. Accordingly, the effect of electron-electron interactions can, at this level, be absorbed in the values of the tight-binding parameters in the undistorted phase.

To conclude, we have shown that a graphene bilayer with A-B stacking can be unstable with respect to a Peierls-type distortion affecting the interplane bonds. This distortion preserves the band structure of the system in the sense that, unlike the original Peierls problem, it does not lead to a gap in the unbiased case nor to its closing in the biased situation. In addition, it was found that the general effect of the bias voltage is to increase the equilibrium deformation.

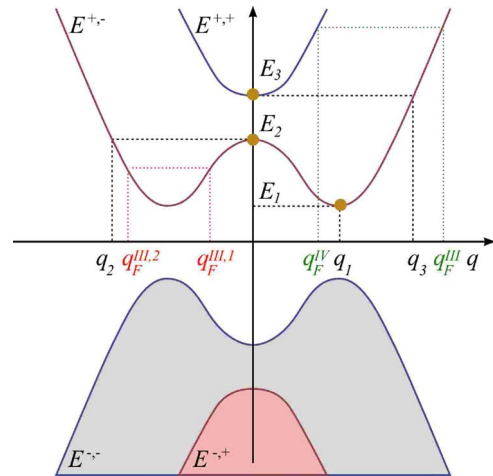


FIG. 7. (Color online) Schematic representation of an arbitrary cut of the band structure of bilayer graphene close to the Dirac point.

ACKNOWLEDGMENTS

V.M.P. is supported by Fundação para a Ciência e a Tecnologia (FCT) via Contract No. SFRH/BPD/27182/2006, and acknowledges Centro de Física do Porto for computational support. N.M.R.P and V.M.P acknowledge the support of POCI 2010 via Contract No. PTDC/FIS/64404/2006. R.M.R. acknowledges the support of FCT under the SeARCH (Services and Advanced Research Computing with HTC/HPC clusters) project (Contract No. CONC-REEQ/443/2005). A.H.C.N. acknowledges the partial support of the U.S. Department of Energy under Grant No. DE-FG02-08ER46512.

APPENDIX A: BAND-STRUCTURE PARAMETERS

With respect to the band structure depicted in Fig. 7, the notable momenta are ($\nu_F = 3ta/2$)

$$q_1 = \frac{1}{2\nu_F} \sqrt{\frac{V^4 + 2V^2 t_\perp^2}{t_\perp^2 + V^2}}, \quad (\text{A1a})$$

$$q_2 = \frac{V}{\nu_F}, \quad (\text{A1b})$$

$$q_3 = \frac{1}{\nu_F} \sqrt{V^2 + 2t_\perp^2}, \quad (\text{A1c})$$

while the corresponding energies are

$$E_1 = \frac{1}{2} \frac{t_\perp V}{\sqrt{V^2 + t_\perp^2}}, \quad (\text{A2a})$$

$$E_2 = \frac{V}{2}, \quad (\text{A2b})$$

$$E_3 = \frac{1}{2} \sqrt{V^2 + 4t_\perp^2}. \quad (\text{A2c})$$

The energy gap is given by

$$\Delta = 2E_1 = \frac{t_\perp V}{\sqrt{V^2 + t_\perp^2}}, \quad (\text{A3})$$

and the midpoint between the upper bands at $q=0$ is at

$$E_{\text{mid}} = \frac{V + \sqrt{V^2 + 4t_\perp^2}}{4}, \quad (\text{A4})$$

to which corresponds the momentum

$$q_{E_{\text{mid}}} = \frac{1}{2\nu_F} \sqrt{V^2 + 4E_{\text{mid}} + 2\sqrt{4E_{\text{mid}}(t_\perp^2 + V^2)} - t_\perp^2 V^2}. \quad (\text{A5})$$

APPENDIX B: ENERGY INTEGRALS

To compute the total electronic energy, the evaluation of the integral

$$F^{\pm, \pm} \equiv \pm \frac{1}{2} \int k dk \sqrt{A + Bk^2 \pm 2\sqrt{D + Ek^2}} \quad (\text{B1})$$

is required. The parameters, with respect to the dispersion of the bilayer in Eq. (6), are given as

$$A = V^2 + 2t_\perp^2, \quad B = 4\nu_F^2, \quad D = t_\perp^4, \quad (\text{B2})$$

$$E = 4\nu_F^2(t_\perp^2 + V^2).$$

The integral is readily computed by changing to the variable $x \equiv \sqrt{D + Ek^2}$, after which it becomes

$$\int x dx \sqrt{\alpha + \beta x + \gamma x^2}, \quad (\text{B3})$$

and is readily available in standard tables. The final result is thus

$$F^{\eta_1, \eta_2} = \frac{\eta_1}{4\nu_F^2(t_\perp^2 + V^2)} \left\{ \frac{R^{3/2}}{3\gamma} - \frac{\gamma x + \eta_2}{2\gamma^2} \eta_2 \sqrt{R} - \frac{\eta_2 \Delta}{8\gamma^{5/2}} \log(2\sqrt{\gamma R} + 2\gamma x + 2\eta_2) \right\}, \quad (\text{B4})$$

where

$$R \equiv \alpha + \beta x + \gamma x^2,$$

$$\Delta \equiv 4\alpha\gamma - \beta^2 = \frac{4V^2 t_\perp^2}{(t_\perp^2 + V^2)^2},$$

$$\alpha \equiv A - \frac{BD}{E} = \frac{V^4 + t_\perp^4 + 3t_\perp^2 V^2}{t_\perp^2 + V^2},$$

$$x \equiv \sqrt{t_\perp^4 + 4\nu_F^2(t_\perp^2 + V^2)k^2},$$

$$\gamma = \frac{1}{t_\perp^2 + V^2},$$

$$\beta = \pm 2. \quad (\text{B5})$$

- ¹A. H. Castro Neto, F. Guinea, N. M. R. Peres, K. S. Novoselov, and A. K. Geim, *Rev. Mod. Phys.* **81**, 109 (2009).
- ²K. S. Novoselov, A. K. Geim, S. V. Morozov, D. Jiang, Y. Zhang, S. V. Dubonos, I. V. Grigorieva, and A. A. Firsov, *Science* **306**, 666 (2004).
- ³K. S. Novoselov, A. K. Geim, S. V. Morozov, D. Jiang, M. I. Katsnelson, I. V. Grigorieva, S. V. Dubonos, and A. A. Firsov, *Nature (London)* **438**, 197 (2005).
- ⁴K. S. Novoselov, D. Jiang, F. Schedin, T. J. Booth, V. V. Khotkevich, S. V. Morozov, and A. K. Geim, *Proc. Natl. Acad. Sci. U.S.A.* **102**, 10451 (2005).
- ⁵A. H. Castro Neto, F. Guinea, and N. M. R. Peres, *Phys. World* **19**, 33 (2006).
- ⁶M. I. Katsnelson and K. S. Novoselov, *Solid State Commun.* **143**, 3 (2007).
- ⁷S. V. Morozov, K. S. Novoselov, M. I. Katsnelson, F. Schedin, D. C. Elias, J. A. Jaszczak, and A. K. Geim, *Phys. Rev. Lett.* **100**, 016602 (2008).
- ⁸K. S. Novoselov, E. McCann, S. V. Morozov, V. I. Fal'ko, M. I. Katsnelson, U. Zeitler, D. Jiang, F. Schedin, and A. K. Geim, *Nat. Phys.* **2**, 177 (2006).
- ⁹T. Ohta, A. Bostwick, T. Seyller, K. Horn, and E. Rotenberg, *Science* **313**, 951 (2006).
- ¹⁰E. McCann, *Phys. Rev. B* **74**, 161403(R) (2006).
- ¹¹E. V. Castro, K. S. Novoselov, S. V. Morozov, N. M. R. Peres, J. M. B. Lopes dos Santos, J. Nilsson, F. Guinea, A. K. Geim, and A. H. Castro Neto, *Phys. Rev. Lett.* **99**, 216802 (2007).
- ¹²J. B. Oostinga, H. B. Heersche, X. Liu, A. F. Morpurgo, and L. M. K. Vandersypen, *Nat. Mater.* **7**, 151 (2008).
- ¹³W. P. Su, J. R. Schrieffer, and A. J. Heeger, *Phys. Rev. Lett.* **42**, 1698 (1979).
- ¹⁴W. P. Su, J. R. Schrieffer, and A. J. Heeger, *Phys. Rev. B* **22**, 2099 (1980).
- ¹⁵C. R. Fincher, D. L. Peebles, A. J. Heeger, M. A. Druy, Y. Matsumura, A. G. MacDiarmid, H. Shirakawa, and S. Ikeda, *Solid State Commun.* **27**, 489 (1978).
- ¹⁶G. M. Rutter, J. N. Crain, N. P. Guisinger, T. Li, P. N. First, and J. A. Stroscio, *Science* **317**, 219 (2007).
- ¹⁷M. S. Dresselhaus and G. Dresselhaus, *Adv. Phys.* **51**, 1 (2002).
- ¹⁸L. Wirtz and A. Rubio, *Solid State Commun.* **131**, 141 (2004).
- ¹⁹H. J. F. Jansen and A. J. Freeman, *Phys. Rev. B* **35**, 8207 (1987).
- ²⁰J. C. Boettger, *Phys. Rev. B* **55**, 11202 (1997).
- ²¹N. Mounet and N. Marzari, *Phys. Rev. B* **71**, 205214 (2005).
- ²²R. J. Nemanich, G. Lucovsky, and S. A. Solin, *Mater. Sci. Eng.* **31**, 157 (1977).
- ²³J.-N. Fuchs and P. Lederer, *Phys. Rev. Lett.* **98**, 016803 (2007).
- ²⁴J. C. Slater and G. F. Koster, *Phys. Rev.* **94**, 1498 (1954).
- ²⁵W. A. Harrison, *Elementary Electronic Structure* (World Scientific, Singapore, 1999).
- ²⁶E.-A. Kim and A. H. Castro Neto, *Europhys. Lett.* **84**, 57007 (2008).
- ²⁷D. A. Papaconstantopoulos, M. J. Mehl, S. C. Erwin, and M. R. Pederson, in *Tight-Binding Approach to Computational Materials Science*, edited by P. Turchi, A. Gonis, and L. Colombo (Materials Research Society, Pittsburgh, 1998), p. 221.
- ²⁸T. Ohta, A. Bostwick, J. L. McChesney, T. Seyller, K. Horn, and E. Rotenberg, *Phys. Rev. Lett.* **98**, 206802 (2007).
- ²⁹L. M. Malard, J. Nilsson, D. C. Elias, J. C. Brant, F. Plentz, E. S. Alves, A. H. Castro Neto, and M. A. Pimenta, *Phys. Rev. B* **76**, 201401(R) (2007).
- ³⁰J. Yan, E. A. Henriksen, P. Kim, and A. Pinczuk, *Phys. Rev. Lett.* **101**, 136804 (2008).
- ³¹M. Lazzeri, C. Attaccalite, L. Wirtz, and F. Mauri, *Phys. Rev. B* **78**, 081406(R) (2008).
- ³²J. P. Perdew, K. Burke, and M. Ernzerhof, *Phys. Rev. Lett.* **77**, 3865 (1996).
- ³³H. J. Monkhorst and J. D. Pack, *Phys. Rev. B* **13**, 5188 (1976).
- ³⁴C. Hartwigsen, S. Goedecker, and J. Hutter, *Phys. Rev. B* **58**, 3641 (1998).
- ³⁵S. Viola Kusminskiy, D. K. Campbell, and A. H. Castro Neto, arXiv:0805.0305 (unpublished).